

# **Empirical models of the monthly and fortnightly ocean tides estimated exclusively from TOPEX/POSEIDON altimetry**

Shailen D. Desai

Jet Propulsion Laboratory, California Institute of Technology, Pasadena

John M. Wahr

Department of Physics and Cooperative Institute for Research in Environmental Sciences, University of Colorado, Boulder

Short title: EMPIRICAL MONTHLY AND FORTNIGHTLY OCEAN TIDES FROM T/P  
ALTIMETRY

**Abstract.** Empirical models for the monthly and fortnightly ocean tides are estimated using sea surface height data from repeat cycles 10 to 190 of the TOPEX/POSEIDON (T/P) altimetry mission. Residual variances between tide gauge observations concentrated in the Pacific Ocean and the presented T/P monthly and fortnightly empirical ocean tide models are both of the order of 2-3 mm<sup>2</sup>. The tide gauge residual variances from the T/P monthly and fortnightly ocean tide models are smaller than those from the respective classical equilibrium ocean tide representations by 0.7 and 8.0 mm<sup>2</sup>, and smaller than those from the respective self-consistent equilibrium ocean tide representations by 1.8 and 15.2 mm<sup>2</sup>, respectively. The principal monthly and fortnightly ocean tide departures from equilibrium are concentrated in the Pacific Ocean where these departures are as large as 3 and 10 mm, respectively. Long-period ocean tide theory predicts that the relative response of the long-period ocean tides approaches equilibrium with increasing period and this is supported by the presented models which show that the observed monthly ocean tide has smaller relative departures from equilibrium than the observed fortnightly ocean tide. The tide gauge comparisons suggest that incoming T/P data will provide improvements to the presented monthly and fortnightly ocean tide models but the most significant improvements are expected in the monthly component. Spherical harmonic decompositions of the presented long-period ocean tide models are provided and these ocean tide models are also used to predict the monthly and fortnightly ocean tide contributions to respective tidal variations of the Earth's rotation rate and polar motion.

## 1. Introduction

The long-period ocean tides have historically been thought to be of sufficiently long period to have frictional effects in the oceans extensively damp the inherent dynamics of the oceans at these periods. The lack of accurate global observations of the long-period ocean tides has precluded any definitive evidence of the extent to which tidal currents at these long periods are actually damped by frictional effects and the long-period ocean tides remain a subject of continuing investigation and speculation. In the extreme case the long-period ocean tides are simply represented by equilibrium theory [*Dahlen, 1976; Agnew and Farrell, 1978*] which assumes that the ocean dynamics at these periods are so severely damped that the long-period ocean tide response coincides, or is in equilibrium, with the forcing equipotential surface. Theoretical and hydrodynamic analyses [e.g. *Proudman, 1959; Carton, 1983*] argue that frictional effects cause tidal currents at periods much longer than the monthly period to be damped to an equilibrium response but that the two principal long-period ocean tide constituents, the monthly  $M_M$  and the fortnightly  $M_f$  constituents, should have departures from equilibrium.

The relatively few accurate tide gauge observations of the monthly and fortnightly ocean tides [e.g. *Miller et al., 1993*] indicate that the departures of these two ocean tides from equilibrium are of the order of less than 1 cm. The small amplitudes of the departures from equilibrium makes them especially difficult to accurately observe. More importantly, the long periods of these ocean tides and the increase in ocean circulation background noise at these periods add to the difficulties involved with observing the long-period ocean tides. The leakage of general ocean circulation noise into observations of the long-period ocean tides is probably the dominant source for errors in these observations [e.g. *Desai et al., 1997*]. Any accurate observations of the long-period ocean tide departures from equilibrium must therefore require long durations of high accuracy data. These observations should ultimately also have global coverage if the observations are to be useful to many applications.

For example, the relative roles that Rossby wave dynamics and gravity waves might have on the  $M_m$  and  $M_f$  ocean tide departures from equilibrium are not completely understood [e.g. *Carton, 1983; Miller et al., 1993; Wunsch et al., 1998*]. Also, equilibrium representations of the  $M_m$  and  $M_f$  ocean tides are incapable of explaining the residual energy at these frequencies in Earth rotation rate observations that have removed the contribution from the solid Earth tides [e.g. *Robertson et al., 1994*]. Most studies of the long-period ocean tides include predictions of their contribution to respective tidal variations of the Earth's rotation rate [e.g. *Agnew and Farrell, 1978; Merriam, 1980; Carton, 1983; Dickman, 1993; Desai, 1996; Kantha et al., 1998*]. If the contribution of the long-period ocean tides and particularly the relative contribution of their departures from equilibrium to tidal variations of the Earth's rotation rate can be accurately determined then the observed variations of the Earth's rotation rate can be used to infer anelastic properties of the Earth's mantle at these tidal frequencies [*Wahr and Bergen, 1986; Desai, 1996*].

Unfortunately, accurate observations of the  $M_m$  and  $M_f$  ocean tides have in most part been limited to relatively few tide gauge observations. However, satellite altimetry serves as an ideal tool to provide almost global observations of the sea surface heights of the Earth's oceans. *Cartwright and Ray [1990]* demonstrated the ability to observe the long-period ocean tides from satellite altimetry by estimating zonally averaged observations of the  $M_f$  ocean tide from Geosat Exact Repeat Mission (ERM) altimetry data, and *Ray and Cartwright [1994]* extended this analysis by using almost two years of Geosat ERM data to estimate zonally averaged observations of both the  $M_m$  and  $M_f$  ocean tides. Their restriction to a zonal analysis was aimed at reducing the effects of oceanographic and altimetric noise caused respectively by the relatively short duration and the large measurement errors in the available Geosat ERM data. Since then the TOPEX/POSEIDON (T/P) altimetry mission has been successfully providing sea surface height measurements of the Earth's oceans with measurement accuracies of the

order of 4-5 cm and the duration of T/P data now extends to over 5 years.

The high accuracy and long duration of the T/P altimetry data provides the first opportunity to develop almost global empirical models of the  $M_m$  and  $M_f$  ocean tides without any restriction to a purely zonal analysis. This has already been demonstrated by *Desai and Wahr* [1995] and *Desai* [1996] who respectively used almost 2 and 3 years of T/P data (repeat cycles 10-78 and 10-110, respectively) to estimate preliminary empirical models of the principal long-period ocean tides with unprecedented spatial resolution. However, these preliminary results from T/P altimetry appeared to contain extensive short wavelength noise in the long-period ocean tide estimates and error analyses by *Desai* [1996] and *Desai et al.* [1997] suggested that longer durations of T/P data would provide improved accuracies to the T/P-derived empirical models of the  $M_m$  and  $M_f$  ocean tides.

Results presented here improve upon earlier results from *Desai and Wahr* [1995] and *Desai* [1996] by using almost 5 years of T/P altimetry data to observe and empirically estimate models for the  $M_m$  and  $M_f$  ocean tides. These most recent results are discussed here at greater length than the previous results and the improved accuracies of these most recent  $M_m$  and  $M_f$  empirical ocean tide models are illustrated through tide gauge comparisons. The present estimates of the global distribution of the  $M_m$  and  $M_f$  departures from equilibrium are shown and zonal averages of these estimates are also provided to illustrate the long wavelength departures from equilibrium. Also discussed are the spherical harmonic decompositions of these empirically observed long-period ocean tides. The T/P  $M_m$  and  $M_f$  ocean tide models are also used to predict their respective contributions to tidal variations of the Earth's rotation rate and polar motion.

## 2. Harmonic Representations of the Ocean Tides

The conventions used by *Desai and Wahr* [1995] are also used here to describe the ocean tides. Those representations that are most relevant to this discussion are

explicitly provided below. The ocean tide response  $\zeta_{nmj}(\theta, \lambda, t)$  at a geographical point with colatitude  $\theta$  and longitude  $\lambda$  of an ocean tide originating with the degree  $n$  and order  $m$  spherical harmonic component of the tide potential is expressed in terms of an amplitude  $A(\theta, \lambda)$  and a Greenwich phase  $G(\theta, \lambda)$ . The long-period ocean tides originate with the zonal component of the tide potential where  $n = 2$  and  $m = 0$ . The index  $j$  denotes the individual tidal components within each tidal band.

$$\zeta_{nmj}(\theta, \lambda, t) = A(\theta, \lambda) \cos(\phi_{nmj}(t) - G(\theta, \lambda)) \quad (1)$$

$$\phi_{nmj}(t) = \omega_{nmj}t + \beta_{nmj} + \delta_{nmj}\pi \quad (2)$$

The reader is referred to equations (3), (4), and (5) from *Desai and Wahr* [1995] for more details about the astronomical arguments  $\omega_{nmj}$ ,  $\beta_{nmj}$ , and  $\delta_{nmj}$ , but Table 1 explicitly provides values of these arguments for some of the principal long-period tidal constituents. The ocean tide response defined in equation (1) is often separated into the inphase  $\zeta^i(\theta, \lambda)$  and quadrature  $\zeta^o(\theta, \lambda)$  tidal components.

Table 1
---------

$$\zeta^i = A(\theta, \lambda) \cos G(\theta, \lambda) \quad (3)$$

$$\zeta^o = A(\theta, \lambda) \sin G(\theta, \lambda) \quad (4)$$

Normalizing the inphase and quadrature tidal components by their respective tide potential amplitudes  $H_{nmj}$  provides a useful method to determine the relative response between ocean tide components within specific tidal bands and subsequently also makes the frequency dependence of the ocean tides much more apparent. To this end the complex ocean tide admittance function  $Z(\omega_{nmj}, \theta, \lambda) = X(\omega_{nmj}, \theta, \lambda) + iY(\omega_{nmj}, \theta, \lambda)$  [e.g. *Cartwright and Ray*, 1990] serves as a useful representation of the ocean tides. For the long-period ocean tides the convention used here to relate the admittance function to the inphase and quadrature components is as follows.

$$\zeta^i(\theta, \lambda) = - |H_{20j}| X(\omega_{20j}, \theta, \lambda) \quad (5)$$

$$\zeta^o(\theta, \lambda) = |H_{20j}| Y(\omega_{20j}, \theta, \lambda) \quad (6)$$

The tide potential amplitudes  $H_{nmj}$  are taken here to be defined as tabulated in *Cartwright and Edden* [1973] and are also provided in Table 1.

### 3. Equilibrium Long-Period Ocean Tides

Equilibrium theory ignores ocean dynamics and assumes that the response of the oceans is coincident, or in equilibrium, with the surface of the forcing potential. Classical equilibrium theory assumes that the long-period ocean tides have a response to the tidal potential only, but *Dahlen* [1976] and *Agnew and Farrell* [1978] introduced the self-consistent equilibrium ocean tide to also include the effects of the self gravitation of the equilibrium ocean tides and the load induced deformations of the ocean floor. The long-period tide potential is a purely zonal function and the respective equilibrium long-period ocean tide response functions are therefore completely determined by only the real components of the admittance function. The classical and self-consistent long-period equilibrium ocean tide admittance functions are defined here by the functions  $\bar{Z} = \bar{X} + i\bar{Y}$  and  $\bar{Z}^s = \bar{X}^s + i\bar{Y}^s$ , respectively, where  $\bar{Y} = \bar{Y}^s = 0$ .

$$\bar{X}(\theta, \lambda) = \mathcal{O}(\theta, \lambda) \left[ \gamma_2 \bar{P}_{20} + \bar{K} \right] \quad (7)$$

$$\bar{X}^s(\theta, \lambda) = \mathcal{O}(\theta, \lambda) \left[ \gamma_2 \bar{P}_{20} + \sum_{n=0}^{\infty} \gamma'_n \alpha_n \bar{X}_n^s + \bar{K}^s \right] \quad (8)$$

The function  $\mathcal{O}(\theta, \lambda)$  is the ocean function of *Munk and Macdonald* [1960] which has a value of 1 over the oceans and 0 over land, and  $\alpha_n = [3/(2n + 1)](\rho_w/\rho_e)$  where  $\rho_w$  and  $\rho_e$  are the mean densities of the ocean and Earth, respectively. The body Love number factor  $\gamma_2 = (1 + k_2 - h_2)$  and load Love number factors  $\gamma'_n = (1 + k'_n - h'_n)$  account for the effect of ocean bottom displacements caused respectively by the body tides and the load tides in the solid Earth and the additional potential that results from these displacements. The functions  $\bar{P}_{nm}(\cos \theta)$  are the normalized associated Legendre functions of degree  $n$  and order  $m$ . Refer to equation (6) of *Desai and Wahr* [1995] for the normalizing factor used here for the Legendre functions. The constants  $\bar{K}$  and  $\bar{K}^s$

are introduced to impose the conservation of mass on the two equilibrium ocean tide admittance functions.

$$\int \bar{X}(\theta, \lambda) \sin \theta d\theta d\lambda = \int \bar{X}^s(\theta, \lambda) \sin \theta d\theta d\lambda = 0 \quad (9)$$

Note that  $\gamma_2$  and  $\gamma'_n$  are the only source for any frequency dependence in the long-period equilibrium admittance functions. There are small frequency dependent effects caused by mantle anelasticity at the long periods [Wahr and Bergen, 1986], but for the most part these are small enough to ignore [e.g. Wahr, 1981]. The long-period equilibrium admittance functions can therefore be assumed to be identical for all of the long-period tidal components.

The self-consistent equilibrium ocean tide is dependent on the load that it exerts on the solid Earth which is represented by the second term in equation (8) where  $\bar{X}_n^s$  are the spherical harmonic components of the self-consistent equilibrium ocean tide  $\bar{X}^s$  itself. Equation (8) is then easily solved through an iterative process that is described by Ray and Cartwright [1994, appendix]. Figure 1 illustrates the global distribution of the classical and self-consistent long-period equilibrium ocean tide admittance functions. The classical equilibrium ocean tide admittance is a purely zonal function over the oceans. The self gravitation and load deformations of the ocean tide introduce some longitudinal variability to the self-consistent equilibrium ocean tide admittance function and also tend to amplify the classical equilibrium ocean tide admittance by approximately 18%.

Figure 1

#### 4. TOPEX/POSEIDON Data Reduction and Analysis

Data from the Version C T/P Merged Geophysical Data Records (MGDRs) [AVISO/Altimetry, 1996] are used to empirically estimate the ocean tide models presented here. Environmental corrections for the range delays caused by the wet and dry troposphere, the ionosphere, and the sea state, and geophysical corrections for the

solid Earth tide, the pole tide, the mean sea surface, and the static inverse barometer response are all applied to the raw T/P MGDR sea surface height data. In addition, a correction for the equilibrium long-period ocean tides originating with the degree 3 tide potential are also applied to the data because the degree 3 tide potential has a monthly component with an amplitude that is of the order of 10% of the amplitude of the principal monthly component of the degree 2 tide potential.

Similar methods to those adopted by *Desai and Wahr* [1995] and *Desai* [1996] are adopted to estimate the T/P  $M_f$  and  $M_m$  empirical ocean tide models and are therefore only summarized here. The ocean tide models are estimated from collinear differences of data from T/P exact repeat cycles that are spaced 2 cycles apart using data from both the solid state altimeter and the dual frequency altimeter from repeat cycles 10 to 190 of the T/P mission. The diurnal and semidiurnal ocean tides are modeled by smooth response functions, and the long-period ocean tides are modeled by three constant response functions that are centered about the monthly  $M_m$ , fortnightly  $M_f$ , and termensual (9 day)  $M_t$  tidal components. The  $M_m$ ,  $M_f$ , and  $M_t$  response functions assume a constant response between 22, 25, and 40 tidal components with frequencies that range from 0.02854986 to 0.04450524 cycles per day (cpd), 0.06286947 to 0.07897221 cpd, and 0.09642334 to 0.14607968 cpd, respectively. The tidal components included in these three long-period tidal bands are chosen to be all of those components defined in the tide-generating potential of *Cartwright and Edden* [1973] that respectively have the same group number as the principal  $M_m$ ,  $M_f$ , and  $M_t$  tidal components, where the group number is the combination of the first two digits of the Doodson number of the individual tidal components. The  $M_t$  tidal band also includes all of those tidal components that have the same group number as the  $M_q$  (7 day) tidal component which has a Doodson number of 093.555. The harmonic response at each of the annual and semiannual frequencies are also simultaneously estimated along with the diurnal, semidiurnal, and long-period tidal response functions. The oceans have a strong

seasonal response to atmospheric forcing at the annual and semiannual frequencies and in the altimetric sea surface height measurements these seasonal responses are indistinguishable from the respective long-period tidal response at these two frequencies. The estimated harmonic response at the annual and semiannual frequencies therefore includes both contributions.

Each of these 7 response functions defined by a total of 22 parameters are simultaneously estimated in geographical bins of size  $360^\circ/127$  in longitude and  $1^\circ$  in latitude, and subsequently smoothed and interpolated to a  $1$  by  $1^\circ$  degree grid. The  $M_f$  and  $M_m$  empirical ocean tide models presented here are therefore only two specific components of an empirical ocean tide model that also includes models for the diurnal and semidiurnal ocean tides. The tidal response functions that are estimated directly from the T/P data actually represent the elastic ocean tides since no load tide corrections were applied to the T/P sea surface height data. The elastic ocean tide refers to the sum total of the pure ocean tide and the associated load tide. The  $1$  by  $1^\circ$  gridded elastic ocean tide estimates are separated into the ocean tide and load tide contributions using the iterative spherical harmonic procedure that is outlined in *Cartwright and Ray* [1991, appendix].

The estimation strategies of *Desai and Wahr* [1995] and *Desai* [1996] summarized above have also been modified in this analysis to allow each altimetric sea surface height observation to contribute to the elastic ocean tide estimates in each of the four surrounding bins. This is accomplished by spatially weighting each data point according to its distance from the center of each bin while ensuring that each sea surface height data point continues to have a unit weight to the global ocean tide model by normalizing the spatially determined weights. Tide gauge comparisons indicate that this strategy provides small improvements to the estimates of the principal semidiurnal ocean tide components, especially the  $M_2$  component, but has little effect on the estimates of the diurnal and long-period ocean tides.

## 5. Tide Gauge Comparisons

The most significant  $M_f$  and  $M_m$  ocean tide departures from equilibrium occur in the Pacific Ocean and the set of 17  $M_m$  and 24  $M_f$  tide gauge observations from *Miller et al.* [1993] which are concentrated in the Pacific Ocean within the longitudes 140°E and 250°E and latitudes 30°S and 30°N provide useful comparisons for the respective ocean tide models that are estimated from T/P altimetry. *Miller et al.* [1993] use long durations (3 to 65 years) of tide gauge data to observe the two principal long-period ocean tides and these long durations should significantly reduce errors in their observations that could have otherwise been caused by oceanographic noise at these long periods. Error estimates are also provided with the *Miller et al.* [1993] tide gauge observations and Figure 2 shows how the T/P tide model estimated from repeat cycles 10 to 190 of the T/P mission, and the two equilibrium ocean tides compare with these tide gauge observations. Note that the tide gauges are numbered in Figure 2 to have increasing tide gauge numbers correspond to decreasing latitudes of the tide gauge locations.

Figure 2

In most cases the T/P models lie within the error bars of the tide gauge observations. However there are some distinct outliers that may possibly be caused by errors in the tide gauge observations themselves. The tide gauge observations at Apia ( $M_m$  tide gauge 15 and  $M_f$  tide gauge 19 in Figure 2) have been designated as “suspicious” by *Miller et al.* [1993] and the large difference with the T/P observations of the  $M_m$  amplitude and  $M_f$  phase certainly suggest that this tide gauge observation may be in error. The tide gauge observation of the  $M_m$  phase at Midway ( $M_m$  tide gauge 1 in Figure 2) has an uncertainty of  $\pm 180^\circ$  and is therefore of limited use in these comparisons. However, the amplitude of the T/P  $M_m$  model agrees to within the error bar associated with the tide gauge observation at Midway. The  $M_m$  tide gauge observation at Noumea ( $M_m$  tide gauge 17 in Figure 2) has an unexplained anomalous phase that is more than  $90^\circ$  out of phase with respect to the T/P model, but again

agrees to within the specified uncertainties of the corresponding observed amplitude.

The convergence of the T/P  $M_m$  and  $M_f$  ocean tides is also illustrated here by comparing the tide gauge observations to T/P models that successively use 10 additional repeat cycles of T/P altimetric data when estimating the ocean tide models, beginning with a model that uses repeat cycles 10 to 50 and ending with a model that uses repeat cycles 10 to 190. Figure 3 shows the residual variances between these 15 T/P tide model estimates and 14  $M_m$  and 23  $M_f$  tide gauge observations from *Miller et al.* [1993]. The anomalous  $M_m$  tide gauge observations at Apia, Midway, and Noumea, and the  $M_f$  tide gauge observations at Apia, are excluded from the computed residual variances. Table 2 provides the root-mean-square (rms) of the differences between the tide gauge observations and the cycle 190 T/P ocean tide models. For clarity it should be mentioned that these convergence figures appear to differ slightly to those from *Desai et al.* [1997] because the T/P long-period ocean tides presented here are smoothed more extensively than they were in the results presented by *Desai et al.* [1997]. This results with much smaller residual variances in the earlier repeat cycle (before cycle 110) T/P models, but with only minimal reductions of the residual variances in the later repeat cycle models.

Figure 3

Table 2

As was also demonstrated by *Desai et al.* [1997], the T/P long-period ocean tide models continue to converge towards the tide gauge observations as longer durations of data are used to estimate these ocean tides. Comparing the residual variances from the cycle 50 and the cycle 190 T/P models shows that the residual variance of the inphase and quadrature components of the  $M_m$  component are respectively reduced from 8.16 to 3.07  $\text{mm}^2$  and 6.27 to 2.27  $\text{mm}^2$ . This represents a respective decrease from 29 to 11% of the observed inphase variance, and 127 to 46% of the observed quadrature variance. The T/P models only begin to reduce the observed  $M_m$  quadrature variance after at least repeat cycles 10 to 70 are used to estimate the empirical models. Similarly the  $M_f$  inphase and quadrature residual variances are reduced from 4.83 to 2.75  $\text{mm}^2$  and 7.21

to  $2.33 \text{ mm}^2$ , or 7 to 4% and 49 to 16% of the respective observed tide gauge variances. The reason for the increase in the residual variance of the  $M_M$  inphase component starting from the cycle 170 model, and the  $M_f$  quadrature component between the cycle 160 and cycle 180 models is not understood. It is however reassuring that the  $M_f$  quadrature residual variance from the cycle 190 model has decreased towards the respective cycle 150 residual variance and is perhaps an indication of future reductions for the  $M_M$  inphase residual variance. Even with these anomalies the cycle 160 to cycle 190  $M_M$  and  $M_f$  residual variances are all still of the order of  $2\text{-}3 \text{ mm}^2$ . Of significance is the fact that with the exception of the anomalous increases in residual variances mentioned above the trends in Figure 3 of decreasing residual variance with increasing data duration suggest further improvements to both the  $M_M$  and  $M_f$  T/P ocean tide models, but especially the  $M_M$  model, from future additions of T/P data.

Also shown in Figure 3 are the tide gauge residual variances with respect to the two equilibrium ocean tides. Of course, since the two equilibrium ocean tides do not have a quadrature component they do not remove any of the observed variance of the quadrature component of the long-period ocean tides. In contrast the T/P long-period ocean tide models are reducing the observed quadrature variance of both the  $M_M$  and  $M_f$  tidal components and therefore provide better representations of the observed departures from equilibrium. For example, although the  $M_M$  inphase residual variance from the cycle 190 T/P model is approximately  $1.2 \text{ mm}^2$  larger than the respective residual variance from the classical equilibrium ocean tide, the cycle 190 T/P model is accounting for approximately  $2.6 \text{ mm}^2$  of the observed  $M_M$  quadrature variance while the classical equilibrium ocean tide cannot account for any of the observed quadrature variance. The phase comparisons in Figures 2 (b) and (d) are also quite significant because the T/P models, and especially the T/P  $M_f$  model, reflect the latitudinal variations in Greenwich phase angle that are observed by the tide gauges. Meanwhile, using the definition provided in equation (1), the equilibrium ocean tides have a

Greenwich phase of  $0^\circ$  at the latitudes of the tide gauge sites since at these latitudes they have a positive inphase component and a zero quadrature component. This implicitly means that the T/P models at the very least reflect the observed latitudinal departures of the  $M_M$  and  $M_f$  ocean tides from the equilibrium response.

Figures 2 (a) and (c) show that the amplitudes from the classical equilibrium ocean tides have smaller differences with the tide gauge observations and the T/P model estimates than do the amplitudes from the self-consistent equilibrium ocean tides. Overall, the T/P  $M_M$  and  $M_f$  tide gauge residual variances are 0.7 and 8.0  $\text{mm}^2$  smaller than those from the respective classical equilibrium ocean tides, and 1.8 and 15.2  $\text{mm}^2$  smaller than those from the respective self-consistent equilibrium ocean tides. The inherent dynamics of the ocean tides are probably acting as an opposing force to the effects of self-gravitation and loading and causing the true long-period tidal response to appear closer to the classical equilibrium response than the self-consistent equilibrium response. This is certainly supported by the fact that the effect of the ocean dynamics is likely to be stronger at the shorter fortnightly period than at the monthly period and therefore causing the much larger differences between the observed  $M_f$  response and its respective self-consistent equilibrium response than in the respective differences for the  $M_M$  component.

## 6. Zonally Averaged Admittance Functions

The long-period equilibrium ocean tides are principally zonal functions and Figure 4 compares the zonal averages of the equilibrium ocean tide admittance functions to the zonal averages of the cycle 190 T/P  $M_M$  and  $M_f$  ocean tide admittance functions. The  $M_M$  real admittance shows better agreement with the classical equilibrium admittance than the self-consistent equilibrium admittance in the southern and northern latitudes, but the opposite is true in the mid-latitudes between  $20^\circ\text{S}$  and  $20^\circ\text{N}$ . In contrast the  $M_f$  real admittance has better agreement with the classical equilibrium admittance in

Figure 4

all latitudes. These results are similar to earlier results from *Desai and Wahr* [1995] and *Desai* [1996]. However, the results from *Desai and Wahr* [1995] and *Desai* [1996] displayed a flattening of the  $M_M$  real admittance south of  $55^\circ\text{S}$  which is not apparent in the results shown here, and for that matter is not apparent in the Geosat results from *Ray and Cartwright* [1994].

The zonal averages of the T/P imaginary admittance functions certainly support long-period tidal theory in that the departures from equilibrium decrease with increasing tidal period, with the  $M_f$  imaginary admittance function having amplitudes that are approximately a factor of 2 times larger than the  $M_M$  imaginary admittance function. Each of the T/P  $M_M$  and  $M_f$  imaginary admittance functions tend towards negative admittances south of  $40^\circ\text{S}$  which increase in magnitude with decreasing tidal period. Of importance also is the fact that the  $M_M$  imaginary admittance function appears to be of slightly smaller amplitude than respective results presented by *Desai and Wahr* [1995] and *Desai* [1996]. This is most probably the result of longer durations of data being able to reduce the effect of background noise at these long periods.

For comparison, the zonal averages of the *Schwiderski* [1980a, b] hydrodynamic models (hereinafter referred to as the SCH models) of the  $M_M$  and  $M_f$  ocean tides are also provided in Figure 4. The T/P and SCH real admittance functions have reasonable agreement in most latitudes. However, in the extreme southern latitudes the T/P  $M_M$  real admittance function is smaller by approximately 5%, and the  $M_f$  real admittance function is larger by approximately 10%, than the respective SCH models. In the extreme northern latitudes the T/P  $M_M$  real admittance does not exhibit the large drop between  $50^\circ\text{N}$  and  $60^\circ\text{N}$  that is apparent in the respective SCH admittance, but instead has a drop at approximately  $62^\circ\text{N}$ . In the extreme northern latitudes the T/P  $M_f$  real admittance is smaller by approximately 10% than the respective SCH admittance.

The zonally averaged T/P  $M_M$  imaginary admittance function is of the order of 0-5% in most of the latitudes and is at least a factor of 2 smaller than the respective SCH

admittance function which is of the order of 3-11% in the same latitudes. These results indicate that the SCH model predicts much larger  $M_m$  departures from equilibrium than are observed by the T/P altimeter. The *Ray and Cartwright* [1994] Geosat results also tend to have smaller  $M_m$  imaginary admittances than the SCH model, but also have a larger drop in the imaginary admittance north of 20°N which is not apparent in the respective T/P admittance function. In contrast to the  $M_m$  imaginary admittance functions, the T/P and SCH  $M_f$  imaginary admittance functions have much better agreement except in two specific regions. The first region is the latitudes between 40°S and 15°S where the T/P  $M_f$  imaginary admittance function is larger by approximately 3-5% than the respective SCH admittance function. The second region is in the latitudes north of 50°N where the T/P models predict a much more gradual decrease of the  $M_f$  imaginary admittance beginning at about 54°N in contrast to the comparatively sharp drop in the respective SCH admittance function at approximately 62°N. The Geosat results from *Ray and Cartwright* [1994] also exhibit similar differences with the SCH model in the  $M_f$  imaginary admittance between 50°S and 15°S, and north of 50°N.

## 7. Spatial Distribution of Departures from Equilibrium

The zonal averages in Figure 4 demonstrate that the T/P  $M_m$  and  $M_f$  real admittance functions are indeed observing the dominant long wavelength zonal distribution that is expected from long-period equilibrium ocean tide theory, but it is the departures from equilibrium that are of particular interest to studies of the long-period ocean tides. The geographical distribution of the departures of the T/P long-period ocean tides from the equilibrium response are illustrated by constructing the vector differences  $\Delta Z(\omega_{20j}, \theta, \lambda)$  between the T/P ocean tides admittance functions  $Z(\omega_{20j}, \theta, \lambda)$  and the self-consistent equilibrium ocean tide admittance  $\bar{Z}^s(\omega_{20j}, \theta, \lambda)$ .

$$\Delta Z(\omega_{20j}, \theta, \lambda) = Z(\omega_{20j}, \theta, \lambda) - \bar{Z}^s(\omega_{20j}, \theta, \lambda) \quad (10)$$

Plate 1 shows both the magnitude of the vector difference  $|\Delta Z(\omega_{20j}, \theta, \lambda)|$ , and the phase of the vector difference  $G_z$ ,

Plate 1

$$G_z(\omega_{20j}, \theta, \lambda) = \pi - \arg(\Delta Z(\omega_{20j}, \theta, \lambda)) \quad (11)$$

where the bias of the phase by  $\pi$  is included only to have  $G_z$  be defined in a similar convention to the Greenwich phase  $G$  [e.g. equation (13) of *Desai and Wahr, 1995*].

Of immediate concern from Plate 1 are the short wavelength features in the departures from equilibrium. Similar plots for the T/P  $M_t$  ocean tide also exhibit short wavelength features. These features tend to become much more extensive as the amplitude of the tidal component becomes smaller with the short wavelength features being most extensive in the  $M_t$  component, reducing somewhat in the  $M_m$  component, and being least extensive in the  $M_f$  component. This is especially obvious when comparing the Pacific Ocean phase angles of the departures from equilibrium where the largest amplitude  $M_f$  component has comparatively evenly distributed phase angles while the  $M_m$  component has extensive short wavelength structure in the phase angle maps. Therefore, these short wavelength features are likely to be caused by the fact that the smaller amplitude ocean tides are more difficult to observe from the available T/P altimetric sea surface height measurements.

The results in Plate 1 do however still provide some insightful results. Foremost is the fact that both the  $M_m$  and  $M_f$  ocean tide departures from the equilibrium occur principally in the Pacific Ocean. Again, it is evident that the departures from equilibrium become smaller with increasing tidal period. The global mean of the magnitude of the vector differences are 6.6 and 8.1% for the  $M_m$  and  $M_f$  ocean tides respectively. In the Pacific Ocean the  $M_m$  departures from equilibrium are mostly of the order of 2-10% while the  $M_f$  departures from equilibrium are mostly of the order of 8-16%. In the Southern Ocean the departures from equilibrium are larger than 14% for the  $M_f$  ocean tide but smaller by at least a factor of two for the  $M_m$  ocean tide in the

same region. Also, the  $M_M$  and  $M_f$  departures from equilibrium have a similar feature of amplitude 2-4% in the Indian Ocean which extends south to the oceans just south of the African and Australian coasts.

The spatial distribution of the  $M_f$  phase angles  $G_z$  compared to those for  $M_M$  probably most clearly demonstrate the similarities in the response of the long-period ocean tide departures from equilibrium in the Pacific and Indian Oceans. Similar Pacific Ocean phase angles are also somewhat apparent in the  $M_t$  component. Plate 1 (c) and (d) also show how the departures from equilibrium have smaller phase angles in the longer period monthly component than in the fortnightly component. The phase of the vector differences with equilibrium are of the order of  $90 - 150^\circ$  for  $M_f$  in almost all of the Pacific Ocean, but the respective phases for  $M_M$  range between  $30 - 120^\circ$ . Also, in the Indian Ocean where the departures from equilibrium are not as significant as in the Pacific Ocean the  $M_M$  phase angles are mostly of the order of  $60 - 90^\circ$  but increase slightly to about  $120^\circ$  for  $M_f$ . Of note is the fact that the  $M_f$  vector differences in the Southern Ocean southwest of Australia are almost in the opposite direction to those in the Pacific Ocean and range from  $-60$  to  $-120^\circ$ .

## 8. Spherical Harmonic Decomposition

The long-period equilibrium ocean tides are dominated by a second degree zonal spherical harmonic component and a comparison with the respective component of the long-period ocean tides observed by T/P provides insight into the principal long wavelength departures from the equilibrium responses. Following the conventions of *Desai and Wahr* [1995], the spherical harmonic decomposition of the long-period ocean tides is expressed as,

$$\zeta_{nmj}(\theta, \lambda, t) = \sum_l \sum_{k=0}^l \sum_{\pm} C_{lk}^{\pm} P_{lk}(\cos \theta) \cos(\phi_{nmj}(t) \pm k\lambda + \chi_{lk}^{\pm}) \quad (12)$$

where equations (28), (29), (34), (35), (36), and (37) from *Desai and Wahr* [1995] relate the spherical harmonic coefficients  $C_{ik}^{\pm}$  and phase lags  $\chi_{ik}^{\pm}$  to the inphase and quadrature components of the ocean tides. Equation (38) from *Desai and Wahr* [1995] also relates the phase angles  $\chi_{ik}^{\pm}$  to the conventions adopted by *Christodoulidis et al.* [1988]. All spherical harmonic decompositions provided here impose the conservation of mass on the ocean tide models by subtracting a constant mass over the global oceans.

The T/P observations are limited to the oceans within the latitudes of  $\pm 66^{\circ}$  and assumptions must be made about the tidal response of the oceans in those polar latitudes not sampled by the T/P altimeter before the T/P models can be decomposed into their spherical harmonic components. Here, the tidal response in these unsampled polar latitudes is assumed to be zero, or modeled by the *Schwiderski* [1980a, b], classical equilibrium, or self-consistent equilibrium ocean tide models (hereinafter referred to as the SCH, CEQU, and SCEQU models). These four variations of the T/P models will be referred to as the T/P only, T/P+SCH, T/P+CEQU, and T/P+SCEQU models, respectively. Figure 5 illustrates the effect on the second degree spherical harmonic coefficients  $C_{20}^{+}$  and  $\chi_{20}^{+}$  of each of these four models from the successive addition of 10 repeat cycles of T/P data into the estimation of the T/P ocean tide models. For comparison, the coefficients from the CEQU and the SCEQU models are also provided in Figure 5. Table 3 then uses the  $C_{20}^{+}$  and  $\chi_{20}^{+}$  estimates from the cycle 150 to cycle 190 T/P tide models to compute statistics on the scatter of these estimates, and Table 4 compares the  $C_{20}^{+}$  and  $\chi_{20}^{+}$  coefficients from the four variations of the repeat cycle 190 T/P long-period ocean tide models to those from some other models.

Figure 5

Table 3

Table 4

The standard deviations provided in Table 3 might be considered as the  $1\sigma$  errors caused by errors in the T/P ocean tide models themselves, while the difference between the mean values from the four variations of the T/P models quantify errors caused by the uncertainties of the tidal response in the polar latitudes not sampled by the T/P altimeter. Errors in the empirical T/P  $M_f$  ocean tide model appear to be at least an

order of magnitude smaller than the uncertainties of the unsampled polar latitude  $M_f$  response. In contrast, errors in the empirical T/P  $M_m$  ocean tide model are of a similar order of magnitude as the uncertainties of the unsampled polar latitude  $M_m$  response.

Although the T/P altimeter samples approximately 94% of the oceans the remaining unsampled regions have a significant impact on the second degree spherical harmonic components of the long-period ocean tides. Accounting for a non-zero tidal response in the unsampled polar latitudes tends to amplify the  $C_{20}^+$  coefficients of the  $M_m$  and  $M_f$  tidal components by at least 34% and 27%, respectively. The respective impact on the phase angles  $\chi_{20}^+$  is most significant in the  $M_f$  component where the phase angles are altered by more than  $3^\circ$ . This significant impact from the unsampled polar latitude oceans can be attributed to the fact that the real admittance  $X(\omega_{20j})$  of the long-period ocean tides in these unsampled latitudes is likely to be dominated by a zonal distribution which is also likely to be of the order of 40-50% and is therefore of larger amplitude than the respective admittance in the oceans that are sampled by T/P.

The  $1\sigma$  scatter of the  $M_f$   $C_{20}^+$  and  $\chi_{20}^+$  coefficients is much smaller than those for the respective  $M_m$  coefficients and is further evidence that the  $M_f$  ocean tide is better determined from T/P altimetry than the  $M_m$  ocean tide. The  $C_{20}^+$  coefficients appear to be nearly constant, as a function of the number of repeat cycles, for  $M_f$  in comparison to the apparent slope for  $M_m$ . It is nevertheless encouraging that the slope of the  $M_m$   $C_{20}^+$  coefficients appears to be decreasing as additional data are included into the tide model estimates, and the  $M_m$   $C_{20}^+$  coefficients appear to be converging towards a value that lies in between those from the classical and self-consistent equilibrium ocean tides.

Figures 5 (a) and (c) support previous results in that the T/P models have a response that is closer to the classical equilibrium response than the self-consistent equilibrium response, and in that the dynamics of the long-period ocean tides tend to act as an opposing force to the effects of self-gravitation and load induced deformations. The effects of self-gravitation and loading tend to amplify both of the  $M_m$  and  $M_f$   $C_{20}^+$

coefficients by 18%, but the effects of the ocean dynamics tend to reduce the amplitude of these coefficients by approximately 8-14% for  $M_m$  and 10-19% for  $M_f$ . These results are again consistent with the expectation that the effect of ocean dynamics should be larger at the shorter fortnightly period than at the monthly period. Since the  $M_m$  departures from equilibrium are smaller than those for  $M_f$ , the phase angles  $\chi_{20}^+$  for  $M_m$  which range from  $175 - 178^\circ$  are closer to the equilibrium values of  $180^\circ$  than are the phase angles for  $M_f$  which range from  $162 - 170^\circ$ .

The zonal averages illustrated in Figure 4 suggest that the long wavelength response of T/P  $M_m$  ocean tide is slightly closer to that of the CEQU model than to those of the SCH and SCEQU models. In contrast the long wavelength response of the T/P  $M_f$  model is closer to that of the SCH model than to those from the equilibrium models. As such, the long wavelength component of the unsampled polar latitude response is probably best approximated by the CEQU model for  $M_m$ , and by the SCH model for  $M_f$ . This is to some extent evident in the results presented in Table 4 where the  $C_{20}^+$  and  $\chi_{20}^+$  coefficients from the SCH and T/P+SCH  $M_f$  models are quite similar in comparison to those from the respective  $M_m$  models.

## 9. Long-Period Tidal Variations of the Earth Rotation Vector

The redistribution of the mass of the oceans due to the ocean tides causes tidal variations in the inertia tensor of the Earth, and the tidal currents cause tidal variations in the relative angular momentum of the oceans with respect to the solid Earth. These variations must be accompanied by corresponding tidal variations of the Earth's rotation vector in order to conserve the angular momentum of the solid Earth and the oceans [e.g. *Wahr, 1982; Gross, 1992*]. These changes to the Earth's rotation vector are observed both by changes in the Earth's rotation rate and polar motion.

Using a body-fixed right-handed coordinate system with x-axis pointing towards the Greenwich meridian, and y-axis towards  $90^\circ\text{E}$ , the small perturbations to the Earth's

inertia tensor are defined by  $c_{ij}(t)$ . Only the elements  $c_{i3}(t)$  ( $i = 1, 3$ ) contribute to tidal variations of the Earth's rotation vector, and these mass contributions are dependent only on the ocean tide heights  $\zeta(\theta, \lambda, t)$  (see equation (1)),

$$\begin{aligned} \mathbf{c}(t) &= c_{13}(t) + ic_{23}(t) \\ &= -\rho_w R^4 \int_0^{2\pi} \int_0^\pi \zeta(\theta, \lambda, t) \sin^2 \theta \cos \theta e^{i\lambda} d\theta d\lambda \end{aligned} \quad (13)$$

$$c_{33}(t) = \rho_w R^4 \int_0^{2\pi} \int_0^\pi \zeta(\theta, \lambda, t) \sin^3 \theta d\theta d\lambda \quad (14)$$

where  $R$  is the mean equatorial radius of the Earth.

The variations of the relative angular momentum of the oceans  $h_i(t)$  ( $i = 1, 3$ ) define the motion contribution to tidal variations of the Earth's rotation vector and are determined from the southward  $u(\theta, \lambda, t)$  and eastward  $v(\theta, \lambda, t)$  tidal currents.

$$\begin{aligned} \mathbf{h}(t) &= h_1(t) + ih_2(t) \\ &= \rho_w R^3 \int_0^{2\pi} \int_0^\pi H(\theta, \lambda) \mathbf{F}(\theta, \lambda, t) \sin \theta d\theta d\lambda \end{aligned} \quad (15)$$

$$h_3(t) = \rho_w R^3 \int_0^{2\pi} \int_0^\pi H(\theta, \lambda) v(\theta, \lambda, t) \sin^2 \theta d\theta d\lambda \quad (16)$$

The complex function  $\mathbf{F}(\theta, \lambda, t)$  is defined as follows.

$$\mathbf{F}(\theta, \lambda, t) = (iu(\theta, \lambda, t) - v(\theta, \lambda, t) \cos \theta) e^{i\lambda} \quad (17)$$

The tidal currents are assumed to be constant through the column of water of depth  $H(\theta, \lambda)$ . Here, the tidal currents are approximated through the application of finite differences of the tide height models into the frictionless Laplace tidal equations [e.g. *Hough and Newton*, 1897], similar to the procedure adopted by *Ray et al.* [1994] and *Chao et al.* [1995] on tide height models of the diurnal and semidiurnal ocean tides. The numerical implementation of the frictionless Laplace tidal equations results with apparent singularities that occur near the equator for the long-period ocean tides. These are overcome through the linear interpolation of the tidal currents across these critical latitudes [e.g. *Ray et al.*, 1994; *Desai*, 1996].

### 9.1. Variations of Earth's Rotation Rate

If  $\Omega$  is defined to be the mean rotation rate of the Earth then the incremental rotation rate  $m_3\Omega$  caused by the ocean tides are interpreted either by variations in the length of day  $\Delta\Lambda$  where  $\Lambda_0 = 86400$  sec is the nominal length of day, or by variations in Universal time UT1 with respect to the reference atomic time standard TAI.

$$m_3 = -\frac{\Delta\Lambda(t)}{\Lambda_0} = \frac{d(\text{UT1-TAI})}{dt} \quad (18)$$

$$\dot{m}_3 = -\dot{\chi}_3 \quad (19)$$

$$\chi_3(t) = \frac{1}{C_m\Omega}[0.756\Omega c_{33}(t) + h_3(t)] \quad (20)$$

The Earth rotation rate excitation function is  $\chi_3$  [Wahr, 1982; Wahr, 1983] where  $C_m$  is the polar moment of inertia of the mantle.

The long-period tidal variations of the Earth's rotation rate are parameterized here in terms of inphase  $UT_s$  and quadrature  $UT_c$  variations in UT1 for each tidal component.

$$(\text{UT1-TAI}) = UT_c \cos(\phi_{nmj}(t)) + UT_s \sin(\phi_{nmj}(t)) \quad (21)$$

Figure 6 illustrates the predicted contributions to variations in UT1 from the T/P+SCH  $M_m$  and  $M_f$  ocean tides as a function of the duration of T/P data used to estimate the T/P tide height models. Tables 5 and 6 then compare the variations in UT1 predicted by the two equilibrium, and the three global variations of the cycle 190 T/P  $M_m$  and  $M_f$  ocean tide models to those from some other studies. It should be mentioned that the two equilibrium models have no motion contributions to variations in UT1 because they implicitly have no tidal currents. Of course, the inphase mass contributions from the long-period ocean tides to UT1 variations represent the largest contributions because  $c_{33}$  is proportional to the second degree zonal spherical harmonic component of the ocean tides and the long-period ocean tides are dominated by an inphase second degree zonal spherical harmonic component.

Also provided in Tables 5 and 6 are the statistics of the scatter in the predicted UT1 variations from the cycle 150-190 T/P+SCH models. The  $1\sigma$  scatter of the predicted

Figure 6

Tables 5 and

UT1 variations for  $M_M$  are almost 3-4 times larger than those for  $M_f$  and the predicted  $M_M$  UT1 variations are therefore not as well determined as those for  $M_f$ . Similarly, the larger scatter of the motion contributions compared to the mass contributions show that the motion contributions are generally not as well determined as the mass contributions. The larger scatter in the motion contributions is likely to be caused by the fact that the short wavelength errors in the T/P ocean tide height models are amplified in the tide height finite differences that are used to compute the tidal currents.

The *Kantha et al.* [1998] model is a hydrodynamic model that assimilates an earlier version of the cycle 130 T/P model presented in this study and tidal currents are a direct product of the applied hydrodynamic equations of motion. Yet, it predicts  $M_f$  motion contributions to UT1 that are within  $3\mu s$  of the respective cycle 190 predictions from this study. In contrast the  $M_M$  motion contributions differ by as much as  $25\mu s$  in the quadrature component. To some extent this demonstrates the remarkable ability to approximate the tidal currents from the linear application of Laplace's tidal equations to a tide height model as long as the tide height model is not significantly corrupted by short wavelength errors. These results of course underscore existing short wavelength errors in the T/P  $M_M$  ocean tide model.

The substitution of the CEQU or SCEQU tides for the SCH tides in the unsampled polar latitudes has a minimal effect of the order of  $3-6\mu s$  on the predicted  $M_M$  UT1 variations. However, the effect on the predicted  $M_f$  UT1 variations is larger and of the order of  $10-15\mu s$ . Since the unsampled polar latitude  $M_M$  and  $M_f$  responses are probably best approximated by the CEQU and SCH models, respectively, the contributions of these two ocean tides on respective tidal variations in UT1 are probably best predicted by values from the T/P+CEQU  $M_M$  and the T/P+SCH  $M_f$  models.

## 9.2. Variations of Polar Motion

*Gross* [1992] notes that observatories located on the surface of the Earth make

observations that more nearly coincide with the motion of the figure axis, rather than the rotation axis, in the body fixed frame. If the reported pole is defined by the complex function  $\mathbf{p}(t) = p_1 + ip_2(t)$  with real ( $p_1$ ) and imaginary ( $p_2$ ) parts that are positive towards  $0^\circ\text{E}$  and  $90^\circ\text{E}$  longitudes, respectively, then the equation of motion that defines  $\mathbf{p}(t)$  is,

$$\mathbf{p}(t) + \frac{i}{\sigma_0} \dot{\mathbf{p}}(t) = \chi(t) \quad (22)$$

$$\chi(t) = \frac{1.61}{(C - A)\Omega} \left[ \frac{\Omega \mathbf{c}(t)}{1.44} + \mathbf{h}(t) \right] \quad (23)$$

where  $\chi(t)$  is the polar motion excitation function [Gross, 1992; Gross, 1993; Wahr, 1982]. The mean polar and equatorial moments of inertia of the Earth are  $C$  and  $A$ , respectively, and  $\sigma_0$  is the Chandler wobble frequency with period  $T = 434.45$  sidereal days and dissipation factor  $Q$  of 170, where  $\sigma_0 = (2\pi/T)[1 + i/2Q]$ . It should be cautioned that equation (22) can only be used to predict polar motion when the excitation function has frequencies that are not close to the free core nutation frequency of  $-1-1/433.2$  cycles per sidereal day, and suffices for predictions of the long-period tidal variations in polar motion.

The reported polar motion is separated into prograde and retrograde components, with amplitudes  $A_p$  and  $A_r$ , and phase lags  $\alpha_p$  and  $\alpha_r$ , respectively [e.g. Gross, 1993],

$$\mathbf{p}(t) = A_p e^{i\alpha_p} e^{i\phi_{nmj}(t)} + A_r e^{i\alpha_r} e^{-i\phi_{nmj}(t)} \quad , \quad (24)$$

Figure 7 illustrates the  $M_m$  and  $M_f$  polar motion predictions. For the sake of clarity only the cycle 150 to cycle 190 T/P+SCH models are shown. Tables 7 and 8 then provide explicit values for the  $M_m$  and  $M_f$  polar motion predictions from the various T/P models, and from the Brosche *et al.* [1989] and Dickman [1993] models.

It is interesting to note how the mass and motion contributions to tidal variations in polar motion are generally perpendicular to each other. Both the prograde and retrograde long-period polar motion components have contributions from the motion

Figure 7

Tables 7 and

component that are of comparable amplitude to the mass component. The motion contributions would be expected to have a larger scatter than the mass contributions because of errors from the short wavelength noise in the T/P models. However, the scatter of the mass and motion contributions are actually quite similar and both of the order of 5 - 10 microarcseconds ( $\mu\text{as}$ ) in amplitude, and of the order of approximately  $10^\circ$  in phase. The exceptions are the predicted  $M_M$  prograde mass, and retrograde motion contributions which appear to have a particularly larger scatter in their phase angles of the order of  $30^\circ$ , but these are probably associated with their much smaller amplitudes.

The polar motion predictions from the various forms of the T/P ocean tide models have amplitudes that are at least a factor of 3 times larger than the predictions from the two equilibrium ocean tide models. Comparison of the predicted polar motion variations from the T/P+SCH models to those from the T/P+CEQU and T/P+SCEQU models provides an indication of the contribution from the tidal heights and currents in the polar latitudes not sampled by T/P. The mass contributions from the unsampled polar latitudes are reduced by more than  $10 \mu\text{as}$  in the  $M_M$  component, and increased by at least  $5 \mu\text{as}$  in the  $M_f$  component when the SCH ocean tides are substituted by the equilibrium ocean tides in the polar latitudes. Meanwhile, the most significant effect of the different polar latitude motion contributions is in the  $M_M$  retrograde predictions which are increased by more than  $20 \mu\text{as}$  when the SCH tides are replaced by the equilibrium tides.

It appears that the polar motion predictions are much more sensitive to the increasing duration of available T/P data than the UT1 predictions, but this is probably caused by the fact that the UT1 predictions are essentially dominated by the principal long-wavelength response of the long-period ocean tides. However, the increasing duration of data has certainly reduced the scatter of the polar motion predictions quite significantly, and even longer durations of T/P data are certainly required to reduce the

uncertainties of both the predicted mass and motion contributions to long-period tidal variations in polar motion. The long-period tidal response in those polar latitudes not sampled by the T/P altimeter are also important to polar motion predictions and cause uncertainties in the polar motion predictions that are of similar or larger amplitude than the uncertainties in the predicted contributions from the T/P models.

## 10. Conclusion

The presented models of the  $M_m$  and  $M_f$  ocean tides that have been estimated from almost 5 years of T/P sea surface height data show that the principal departures of the long-period ocean tide response from an equilibrium response occur in the Pacific Ocean. Comparisons of the T/P models to tide gauge observations that are concentrated in the Pacific Ocean show that the tide gauge residual variances from the T/P models are smaller than from either of the respective classical or self-consistent equilibrium ocean tides. Since the equilibrium ocean tides do not have a quadrature component a significant portion of the smaller residual variances from the T/P models than from the equilibrium models is due to the ability of the T/P models to observe the quadrature component of these two long-period ocean tides.

Tidal theories have predicted that the long-period ocean tide departures from equilibrium decrease with increasing tidal period and this is supported by the fact that the T/P models observe smaller relative departures from equilibrium in the  $M_m$  component than in the  $M_f$  component. The T/P  $M_m$  and  $M_f$  ocean tide models show better agreement with the classical equilibrium ocean tide than the self-consistent equilibrium ocean tide but this phenomenon is most likely caused by the opposing effect of the ocean dynamics with respect to the effects of self-gravitation and loading. The T/P  $M_f$  ocean tide shows similar long-wavelength departures from equilibrium as does the respective *Schwiderski* [1980a, b] model. In contrast, the T/P  $M_m$  model shows significantly smaller departures from equilibrium than does the respective *Schwiderski*

[1980a, b] model, and the T/P  $M_m$  model might even be considered to have a response that is closer to the respective classical equilibrium ocean tide than it is to the respective *Schwiderski* [1980a, b] ocean tide.

A comparison of the presented models to earlier versions from *Desai and Wahr* [1995] and *Desai* [1996] demonstrates how using longer durations of T/P data to empirically estimate models for the  $M_m$  and  $M_f$  ocean tides tends to reduce the extent and magnitude of short wavelength errors in these models. These short wavelength errors are still quite apparent in the T/P  $M_m$  empirical ocean tide models. Fortunately, the presented tide gauge comparisons also suggest that future additions of incoming T/P data are likely to provide further improvements to both of these ocean tide models, but especially to the  $M_m$  ocean tide model.

The uncertainties of the  $M_m$  and particularly the  $M_f$  ocean tides in the polar latitudes not sampled by the T/P altimeter appear to be the dominant source for errors in some global applications of these two long-period ocean tides, such as spherical harmonic decompositions and predictions of the contributions that these ocean tides have on tidal variations of the Earth's rotation rate. In the case of polar motion predictions, the uncertainties in the contribution from the tidal response in these unsampled polar latitudes appear to be of a similar order of magnitude as the uncertainties from the contributions predicted by the T/P models. However, the classical equilibrium  $M_m$  and *Schwiderski* [1980a, b]  $M_f$  ocean tides probably serve as reasonable approximations of the respective long wavelength tidal responses in those latitudes not sampled by the T/P altimeter until better models become available.

The extensive short wavelength errors in the T/P  $M_m$  ocean tide models are also a large source of errors in the predictions of the contribution that the  $M_m$  tidal currents have on tidal variations of the Earth's rotation rate. Of course, incoming T/P data should also reduce the magnitude of these errors as the extent of the short wavelength errors is reduced. Except for the uncertainties in the unsampled polar latitude tidal

response, predictions of the effect that the  $M_f$  ocean tide has on respective tidal variations of the Earth's rotation rate appear to be relatively well determined to within a few microseconds from the presented T/P model. The most significant improvements in the Earth rotation rate predictions that might be expected from future updates of the T/P  $M_f$  model are likely to be in the form of improved predictions of the motion contribution. In contrast, the scatter of the mass and motion contributions to polar motion predictions from the T/P long-period ocean tide models are of similar order, and both contributions are likely to benefit from future updates of the T/P long-period ocean tide models.

**Acknowledgments.** Early portions of this work were supported by the TOPEX project at the Jet Propulsion Laboratory under contract 958126 to the University of Colorado. S. D. was also supported by a contract from NASA to the Jet Propulsion Laboratory.

## References

- Agnew, D. C., and W. E. Farrell, Self-consistent equilibrium ocean tides, *Geophys. J. R. Astron. Soc.*, *55*, 171-181, 1978.
- AVISO/Altimetry, AVISO User Handbook for Merged TOPEX/POSEIDON products, AVI-NT-02-101, Edition 3.0, 1996.
- Brosche, P., U. Seiler, J. Sundermann, and J. Wunsch, Period changes in Earth's rotation due to oceanic tides, *Astron. Astrophys.*, *220*, 318-320, 1989.
- Carton, J. A., The variation with frequency of the long-period tides, *J. Geophys. Res.*, *88*(C12), 7563-7571, 1983.
- Cartwright, D. E., and A. C. Edden, Corrected tables of tidal harmonics, *Geophys. J. R. Astron. Soc.*, *33*, 253-264, 1973.
- Cartwright, D. E., and R. D. Ray, Observations of the Mf ocean tide from Geosat altimetry, *Geophys. Res. Lett.*, *17*(5), 619-622, 1990.
- Cartwright, D. E., and R. D. Ray, Energetics of global ocean tides from Geosat altimetry, *J. Geophys. Res.*, *96*(C9), 16,897-16,912, 1991.
- Chao, B. F., R. D. Ray, and G. D. Egbert, Diurnal/ Semidiurnal oceanic tidal angular momentum: Topex/Poseidon models in comparison with Earth's rotation rate, *Geophys. Res. Lett.*, *22*, 1993-1996, 1995.
- Christodoulidis, D. C., D. E. Smith, R. G. Williamson, and S. M. Klosko, Observed tidal braking in the Earth /Moon/Sun system, *J. Geophys. Res.*, *93*(B6), 6216-6236, 1988.
- Dahlen, F. A., The passive influence of the oceans upon the rotation of the Earth, *Geophys. J. R. Astron. Soc.*, *46*, 363-406, 1976.
- Desai, S. D., Ocean tides from TOPEX/POSEIDON altimetry with some geophysical applications, Ph.D. thesis, Univ. of Colo., Boulder, 1996.
- Desai, S. D., and J. M. Wahr, Empirical ocean tide models estimated from TOPEX/POSEIDON altimetry, *J. Geophys. Res.*, *100*(C12), 25,205-25,228, 1995.
- Desai, S. D., J. M. Wahr, and Y. Chao, Error analysis of empirical ocean tide models estimated from TOPEX/POSEIDON altimetry, *J. Geophys. Res.*, *102* (C11), 25,157-25,172, 1997.

- Dickman, S. R., Dynamic ocean-tide effects on Earth's rotation, *Geophys. J. Int.*, *112*, 448-470, 1993.
- Gross, R. S., Correspondence between theory and observations of polar motion, *Geophys. J. Int.*, *109*, 162-170, 1992.
- Gross, R. S., The effect of ocean tides on the Earth's rotation as predicted by the results of an ocean tide model, *Geophys. Res. Lett.*, *20*(4), 293-296, 1993.
- Hough, S. S., and I. Newton, On the application of harmonic analysis to the dynamical theory of the tides. - Part I. On Laplace "oscillations of the first species", and on the dynamics of the ocean currents, *Phil. Trans. R. Astron. Soc.*, *A189*, 201-257, 1897.
- Kantha, L. H., S. Stewart, and S. D. Desai, Long period lunar fortnightly and monthly ocean tides, *J. Geophys. Res.*, in press, 1998.
- Lerch, F. J., et al., Geopotential models of the Earth from satellite tracking, altimeter and surface gravity observations: GEM-T3 and GEM-T3s, *NASA Tech. Memo. 104555*, 1992.
- Merriam, J. B., Zonal tides and changes in the length of day, *Geophys. J. R. Astron. Soc.*, *62*, 551-561, 1980.
- Miller, A. J., D. S. Luther, and M. C. Hendershott, The fortnightly and monthly tides: Resonant Rossby waves or nearly equilibrium gravity waves?, *J. Phys. Oceanogr.*, *23*, 879-897, 1993.
- Munk, W. H., and G. J. F. Macdonald, *The Rotation of the Earth, A Geophysical Discussion*, Cambridge Univ. Press, New York, 1960.
- Proudman, J., The condition that a long-period tide shall follow the equilibrium law, *Geophys. J. R. Astron. Soc.*, *3*, 244-249, 1959.
- Ray, R. D., and D. E. Cartwright, Satellite altimeter observations of the Mf and Mm ocean tides, with simultaneous orbit corrections, *Gravimetry and Space Techniques Applied to Geodynamics and Ocean Dynamics*, *Geophys. Monogr. Ser. 82*, vol 17, edited by B. E. Schutz et al., pp 69-78, AGU, Washington, D. C., 1994.
- Ray, R. D., D. J. Steinberg, B. F. Chao, and D. E. Cartwright, Diurnal and semidiurnal variations of the Earth's rotation rate induced by oceanic tides, *Science*, *264*, 830-832,

1994.

- Robertson, D. S., J. R. Ray, and W. E. Carter, Tidal variations in UT1 observed with very long baseline interferometry, *J. Geophys. Res.*, *99*(B1), 621-636, 1994.
- Schwiderski, E. W., Ocean tides, I, Global ocean tide equations, *Mar. Geod.*, *3*, 161-217, 1980a.
- Schwiderski, E. W., Ocean tides, II, A hydrodynamical interpolation model, *Mar. Geod.*, *3*, 219-255, 1980b.
- Wahr, J. M., Body tides on an elliptical, rotating, elastic and oceanless Earth, *Geophys. J. R. Astron. Soc.*, *64*, 677-703, 1981.
- Wahr, J. M., The effects of the atmosphere and oceans on the Earth's wobble -I. Theory, *Geophys. J. R. Astron. Soc.*, *70*, 349-372, 1982.
- Wahr, J. M., The effects of the atmosphere and oceans on the Earth's wobble and on seasonal variations in the length of day - II. Results, *Geophys. J. R. Astron. Soc.*, *74*, 451-487, 1983.
- Wahr, J. M., and Z. Bergen, The effects of mantle anelasticity on nutations, Earth tides, and tidal variations in rotation rate, *Geophys. J. R. Astron. Soc.*, *87*, 633-668, 1986.
- Wunsch, C., D. B. Haidvogel, M. Iskandarani, and R. Hughes, Dynamics of the long-period tides, *Progress in Oceanography*, 1998.

---

S. D. Desai, Jet Propulsion Laboratory, California Institute of Technology, Mail Stop 238-600, 4800 Oak Grove Drive, Pasadena, CA 91109. (e-mail: Shailen.D.Desai@jpl.nasa.gov)

J. M. Wahr, Department of Physics, Campus Box 390, University of Colorado, Boulder, CO 80309-0390. (e-mail: wahr@longo.colorado.edu)

Received May 11, 1998

Paper Submitted to *J. of Geophysical Research - Oceans*, 1998

**Table 1.** Long-Period Tidal Arguments

Tide	Doodson Number	$H_{20j}$ cm	$\omega_{20j}$ cpd	$\beta_{20j}$ <sup>a</sup> deg	$\delta_{20j}$
S <sub>a</sub>	056.554	-0.492	0.0027377786	357.5252	0
S <sub>sa</sub>	057.555	-3.098	0.0054758187	200.9306	0
M <sub>m</sub>	065.455	-3.518	0.0362916471	134.9754	0
M <sub>f</sub>	075.555	-6.661	0.0732022027	76.6502	0
M <sub>t</sub>	085.455	-1.276	0.1094938498	211.6256	0
M <sub>q</sub>	093.555	-0.204	0.1409285867	312.3699	0

The cpd refers to cycles per solar day.

<sup>a</sup>The astronomical phase angles are referenced to noon on Jan 1, 2000 with a Modified Julian Date of 51544.5 days.

**Table 2.** Root-Mean-Square of Differences Between 14  $M_m$  and 23  $M_f$  Tide Gauge Observations from *Miller et al.* [1993] and the Respective Classical Equilibrium, Self-Consistent Equilibrium, and the T/P Cycle 190 Ocean Tides.

Model	$M_m$ Tide			$M_f$ Tide		
	Inphase	Quadrature	Total	Inphase	Quadrature	Total
No Model	5.28	2.22	4.05	8.20	3.83	6.40
Self-Consistent Equilibrium	2.04	2.22	2.13	4.55	3.83	4.21
Classical Equilibrium	1.37	2.22	1.84	2.52	3.83	3.24
TOPEX/POSEIDON Cycle 190	1.75	1.51	1.64	1.66	1.52	1.59

Units are millimeters.

**Table 3.** Mean and Standard Deviation of the Second Degree Spherical Harmonic Component Amplitudes  $C_{20}^+$  and Phase Lags  $\chi_{20}^+$  of the Four Variations of the TOPEX/POSEIDON  $M_m$  and  $M_f$  Ocean Tide Models.

Model	$M_m$ Tide				$M_f$ Tide			
	$C_{20}^+$ (cm)		$\chi_{20}^+$ (°)		$C_{20}^+$ (cm)		$\chi_{20}^+$ (°)	
	Mean	$\sigma$	Mean	$\sigma$	Mean	$\sigma$	Mean	$\sigma$
T/P Only	0.741	0.018	176.3	0.8	1.415	0.003	166.6	0.3
T/P+SCH	1.008	0.017	178.1	0.5	1.805	0.003	162.2	0.2
T/P+CEQU	1.025	0.017	176.8	0.5	1.921	0.004	169.6	0.2
T/P+SCEQU	1.065	0.017	176.9	0.5	1.995	0.004	170.0	0.2

T/P is TOPEX/POSEIDON. SCH is the *Schwiderski* [1980a, b] ocean tide model. CEQU is the classical equilibrium ocean tide model. SCEQU is the self-consistent equilibrium ocean tide model.  $\sigma$  is the standard deviation about the mean. The mean and standard deviation are computed using values from the repeat cycle 150, 160, 170, 180, and 190 T/P tide models.

**Table 4.** Second Degree Spherical Harmonic Component Amplitudes  $C_{20}^+$  and Phase Lags  $\chi_{20}^+$  of the Long-Period Ocean Tides

Model	M <sub>m</sub> Tide		M <sub>f</sub> Tide	
	$C_{20}^+$ (cm)	$\chi_{20}^+$ (°)	$C_{20}^+$ (cm)	$\chi_{20}^+$ (°)
Classical Equilibrium (CEQU)	0.993	180.0	1.879	180.0
Self-consistent Equilibrium (SCEQU)	1.170	180.0	2.216	180.0
<i>Schwiderski</i> [1980a, b]	1.063	168.9	1.705	162.0
GEM-T3, <i>Lerch et al.</i> [1992]	0.843	170.1	2.052	150.4
T/P Only	0.789	174.9	1.445	166.2
T/P + SCH	1.027	177.3	1.804	162.3
T/P + CEQU	1.044	176.1	1.920	169.7
T/P + SCEQU	1.084	176.2	1.994	170.0

Values for the TOPEX/POSEIDON (T/P) models are taken from the models that are estimated from repeat cycles 10 to 190 of the T/P mission.

**Table 5.** Contribution of the  $M_m$  Ocean Tide to Tidal Variations in UT1

Model	Mass		Motion		Total	
	$UT_c$	$UT_s$	$UT_c$	$UT_s$	$UT_c$	$UT_s$
T/P+SCH (Mean)	3.9 (1.1)	-116.3 (1.9)	27.9 (3.5)	-4.0 (5.9)	31.8 (4.3)	-120.3 (7.4)
T/P+SCH (Cycle 190)	5.6	-118.4	34.9	-15.1	40.5	-133.5
T/P+CEQU	8.2	-120.2	35.7	-14.4	43.9	-134.6
T/P+SCEQU	8.2	-124.8	35.7	-14.4	43.9	-139.2
T/P Only	8.2	-90.6	35.7	-14.4	43.9	-105.0
CEQU	0.0	-114.7	0.0	0.0	0.0	-114.7
SCEQU	0.0	-135.3	0.0	0.0	0.0	-135.3
<i>Brosche et al.</i> [1989] <sup>a</sup>	19.8	-105.0	5.4	0.1	25.2	-105.1
<i>Dickman</i> [1993]	13.1	-125.4	-1.0	-0.3	12.1	-125.7
<i>Kantha et al.</i> [1998]	8.8	-119.1	10.7	5.7	19.4	-113.4

Units are microsec. The mean T/P+SCH values are computed from the cycle 150-190 values.

Values in ()s are the standard deviations about the mean values.

<sup>a</sup>Values are from *Gross* [1993] based on the tide model by *Brosche et al.* [1989].

**Table 6.** Contribution of the  $M_f$  Ocean Tide to Tidal Variations in UT1

Model	Mass		Motion		Total	
	$UT_c$	$UT_s$	$UT_c$	$UT_s$	$UT_c$	$UT_s$
T/P+SCH (Mean)	31.6 (0.4)	-98.3 (0.3)	14.8 (0.9)	-3.8 (0.9)	46.4 (1.2)	-102.1 (0.9)
T/P+SCH (Cycle 190)	31.4	-98.3	14.3	-3.8	45.7	-102.1
T/P+CEQU	19.7	-108.0	13.9	-4.9	33.6	-112.9
T/P+SCEQU	19.7	-112.4	13.9	-4.9	33.6	-117.3
T/P Only	19.7	-80.2	13.9	-4.9	33.6	-85.1
CEQU	0.0	-107.7	0.0	0.0	0.0	-107.7
SCEQU	0.0	-127.0	0.0	0.0	0.0	-127.0
<i>Brosche et al.</i> [1989] <sup>a</sup>	24.7	-87.4	10.2	1.4	34.9	-86.0
<i>Dickman</i> [1993]	22.4	-108.4	-1.7	-0.9	20.7	-109.3
<i>Kantha et al.</i> [1998]	33.0	-102.8	15.4	-1.4	48.5	-104.2

Units are microsec. The mean T/P+SCH values are computed from the cycle 150-190 values. Values in ()s are the standard deviations about the mean values.

<sup>a</sup>Values are from *Gross* [1993] based on the tide model by *Brosche et al.* [1989].

**Table 7.** Contribution of the  $M_M$  Ocean Tide to Tidal Variations in Polar Motion

Model	Prograde						Retrograde					
	Mass		Motion		Total		Mass		Motion		Total	
	$A_p$ ( $\mu\text{as}$ )	$\alpha_p$ ( $^\circ$ )	$A_p$ ( $\mu\text{as}$ )	$\alpha_p$ ( $^\circ$ )	$A_p$ ( $\mu\text{as}$ )	$\alpha_p$ ( $^\circ$ )	$A_r$ ( $\mu\text{as}$ )	$\alpha_r$ ( $^\circ$ )	$A_r$ ( $\mu\text{as}$ )	$\alpha_r$ ( $^\circ$ )	$A_r$ ( $\mu\text{as}$ )	$\alpha_r$ ( $^\circ$ )
T/P+SCH (Mean)	23 (5)	133 (31)	72 (8)	199 (8)	81 (20)	186 (5)	53 (10)	118 (8)	19 (7)	21 (32)	56 (6)	99 (4)
T/P+SCH (Cycle 190)	21	128	79	201	88	188	38	133	31	39	47	93
T/P+CEQU	6	88	76	190	75	186	26	161	54	12	34	36
T/P+SCEQU	2	126	76	190	77	188	27	153	54	12	37	39
T/P Only	30	74	76	190	69	166	34	200	54	12	21	358
CEQU	14	155	0	0	14	155	12	335	0	0	12	335
SCEQU	16	162	0	0	16	162	14	342	0	0	14	342
<i>Brosche et al.</i> [1989] <sup>a</sup>	8	264	46	253	53	254	36	65	34	349	55	28
<i>Dickman</i> [1993]	36	327	8	197	32	316	21	7	6	228	17	354

$\mu\text{as}$  is microarcsec. The mean T/P+SCH values are computed from the cycle 150-190 values.

Values in ( )s are the standard deviations about the mean values.

<sup>a</sup>Values are from *Gross* [1993] based on the tide model by *Brosche et al.* [1989].

**Table 8.** Contribution of the  $M_f$  Ocean Tide to Tidal Variations in Polar Motion

Model	Prograde						Retrograde					
	Mass		Motion		Total		Mass		Motion		Total	
	$A_p$ ( $\mu\text{as}$ )	$\alpha_p$ ( $^\circ$ )	$A_p$ ( $\mu\text{as}$ )	$\alpha_p$ ( $^\circ$ )	$A_p$ ( $\mu\text{as}$ )	$\alpha_p$ ( $^\circ$ )	$A_r$ ( $\mu\text{as}$ )	$\alpha_r$ ( $^\circ$ )	$A_r$ ( $\mu\text{as}$ )	$\alpha_r$ ( $^\circ$ )	$A_r$ ( $\mu\text{as}$ )	$\alpha_r$ ( $^\circ$ )
T/P+SCH (Mean)	45 (6)	1 (8)	34 (6)	269 (15)	55 (11)	323 (10)	91 (6)	34 (5)	42 (7)	308 (6)	104 (14)	11 (6)
T/P+SCH (Cycle 190)	36	14	28	289	48	338	85	43	34	304	86	20
T/P+CEQU	41	356	31	314	66	338	98	42	29	299	96	25
T/P+SCEQU	40	351	31	314	67	335	101	43	29	299	98	26
T/P Only	51	21	31	314	69	357	80	34	29	299	82	14
CEQU	12	155	0	0	12	155	12	335	0	0	12	335
SCEQU	15	162	0	0	15	162	14	342	0	0	14	342
<i>Brosche et al.</i> [1989] <sup>a</sup>	4	263	53	233	56	235	37	116	31	17	44	72
<i>Dickman</i> [1993]	44	299	14	189	41	280	57	13	6	238	53	8

$\mu\text{as}$  is microarcsec. The mean T/P+SCH values are computed from the cycle 150-190 values.

Values in ( )s are the standard deviations about the mean values.

<sup>a</sup>Values are from *Gross* [1993] based on the tide model by *Brosche et al.* [1989].

**Figure 1.** Static long-period equilibrium ocean tide admittances with mass conserved. (a) is the classical equilibrium admittance  $\bar{X}(\theta, \lambda)$ , and (b) is the self-consistent equilibrium admittance  $\bar{X}^s(\theta, \lambda)$ . Dashed contours are negative and the units are percent.

**Figure 2.** Comparison of the 17  $M_M$  and 25  $M_f$  tide gauge observations from *Miller et al.* [1993] to the respective cycle 190 T/P ocean tide models, the classical equilibrium ocean tides (CEQU), and the self-consistent equilibrium ocean tides (SCEQU). (a) and (b) compare the  $M_M$  amplitude and phase, and (c) and (d) compare the  $M_f$  amplitude and phase.

**Figure 3.** Residual variance between 14  $M_M$  and 23  $M_f$  tide gauge observations from *Miller et al.* [1993] and the respective cycle 50 to cycle 190 empirical ocean tide models estimated from T/P altimetric data, the classical equilibrium ocean tides, and the self-consistent equilibrium ocean tides. The residual variances are shown on a logarithmic scale.

**Figure 4.** Zonal averages of the  $M_M$  and  $M_f$ , ocean tide admittance functions from the cycle 190 TOPEX/POSEIDON model, the *Schwiderski* [1980a, b] model, the classical equilibrium ocean tide, and the self-consistent equilibrium ocean tide model.

**Figure 5.** Second degree zonal spherical harmonic components of the  $M_M$  and  $M_f$  ocean tides. SCEQU and CEQU are results from the self-consistent equilibrium and classical equilibrium ocean tides, respectively. T/P+SCH, T/P+SCEQU, and T/P+CEQU are results from ocean tide models created using the TOPEX/POSEIDON models within the latitudes of  $\pm 66^\circ$  and the *Schwiderski* [1980a, b], self-consistent equilibrium, and classical equilibrium ocean tides, respectively, in all other latitudes. The coefficients are computed after imposing the conservation of mass on each ocean tide model.

**Figure 6.** Matter, motion, and total contribution of the T/P+SCH  $M_M$  and  $M_f$  ocean tide models to tidal variations in UT1.

**Figure 7.** Matter, motion, and total contribution to prograde and retrograde polar motion from the cycle 150 to cycle 190 T/P+SCH  $M_M$  and  $M_f$  ocean tide models.

**Plate 1.** Amplitude  $|\Delta Z(\omega_{20j}, \theta, \lambda)|$  and phase  $G_z = [\pi - \arg(\Delta Z(\omega_{20j}, \theta, \lambda))]$  of the vector difference between the T/P monthly  $M_m$  and fortnightly  $M_f$  ocean tide admittance functions and the respective self-consistent equilibrium ocean tide admittance function.

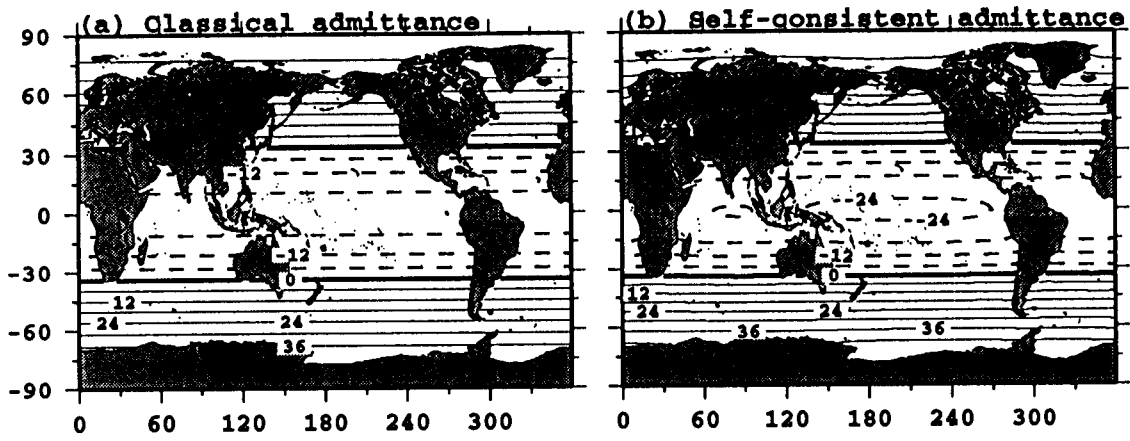


Figure 1.

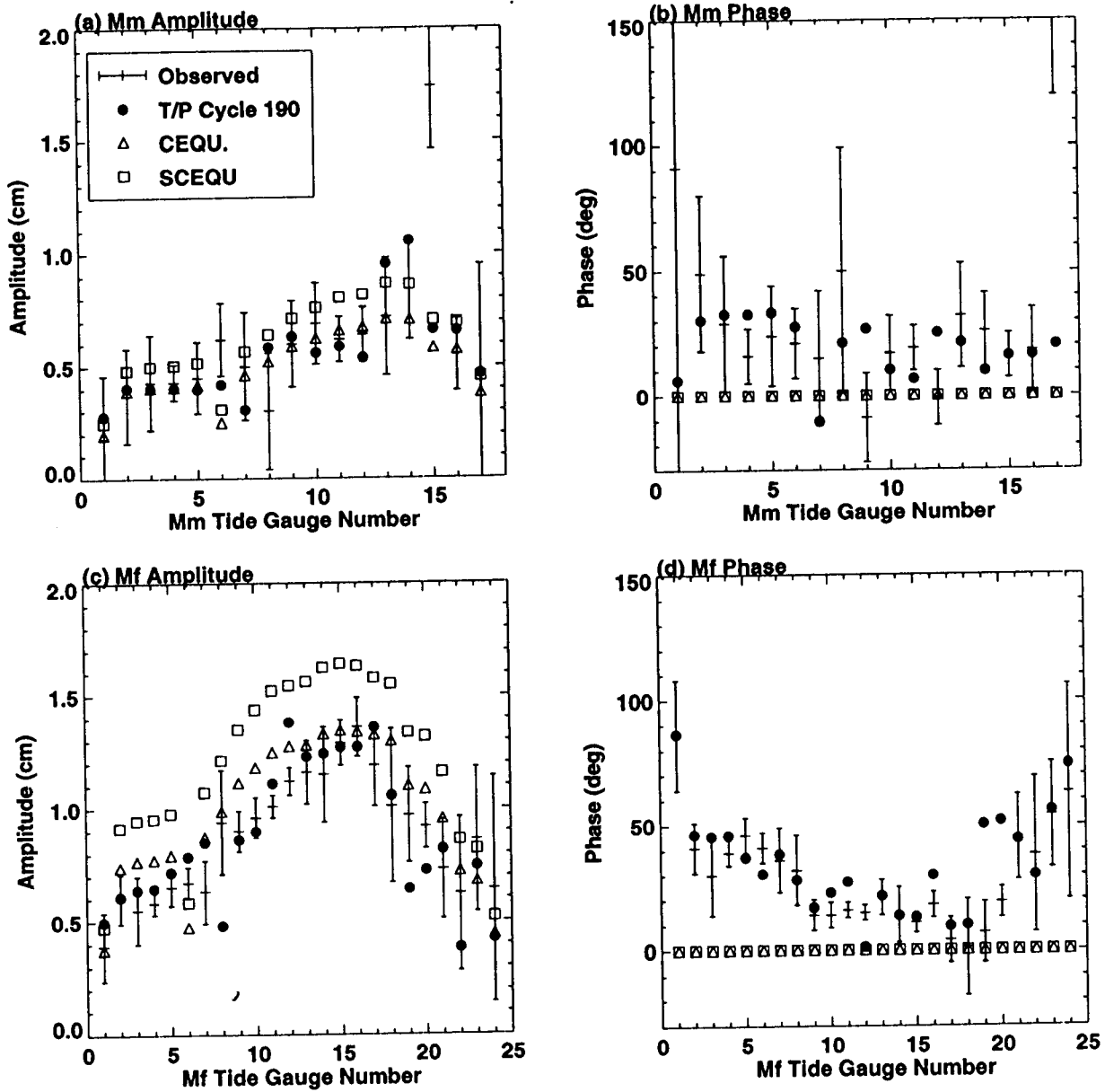


Figure 2.

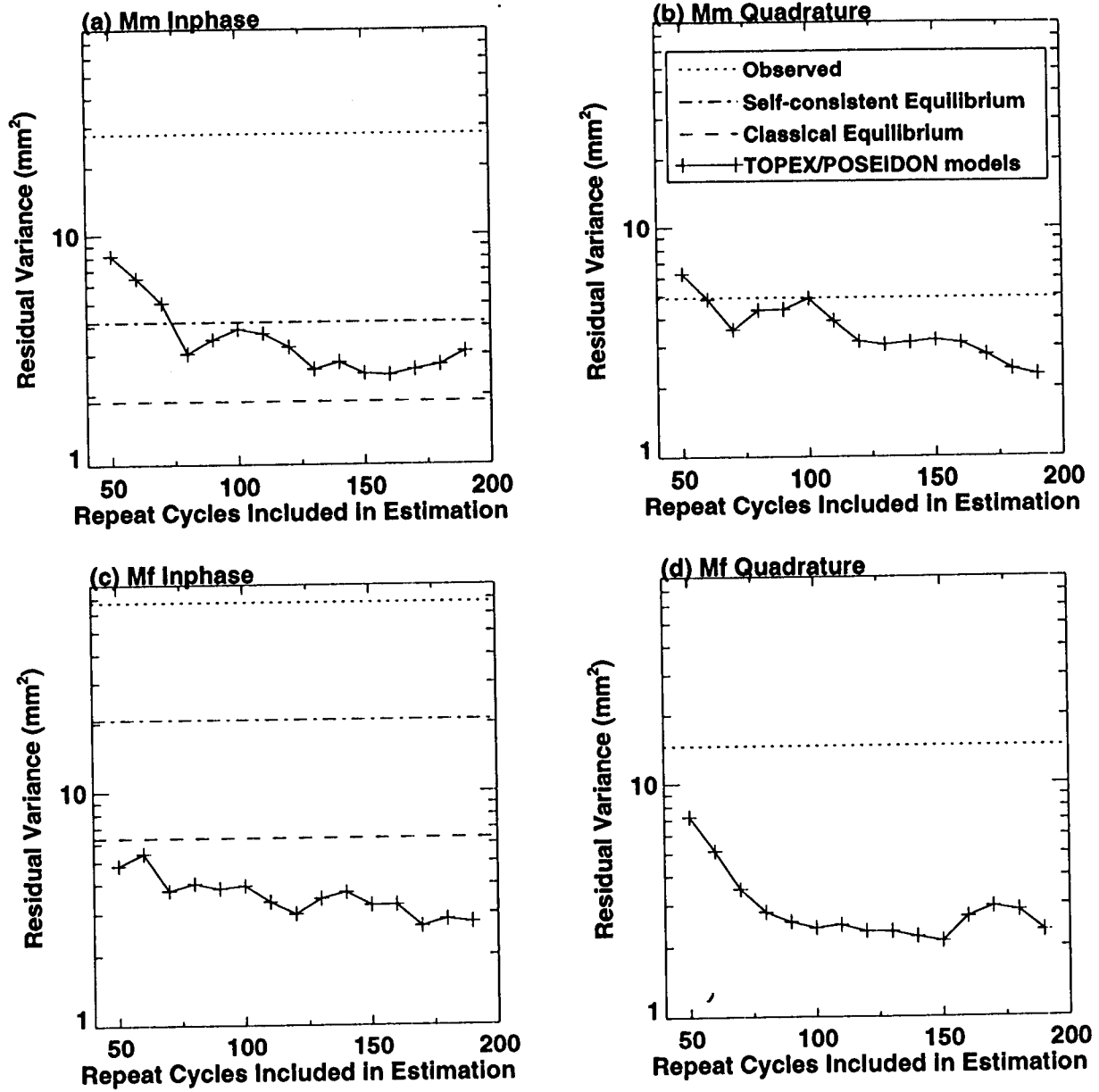


Figure 3.

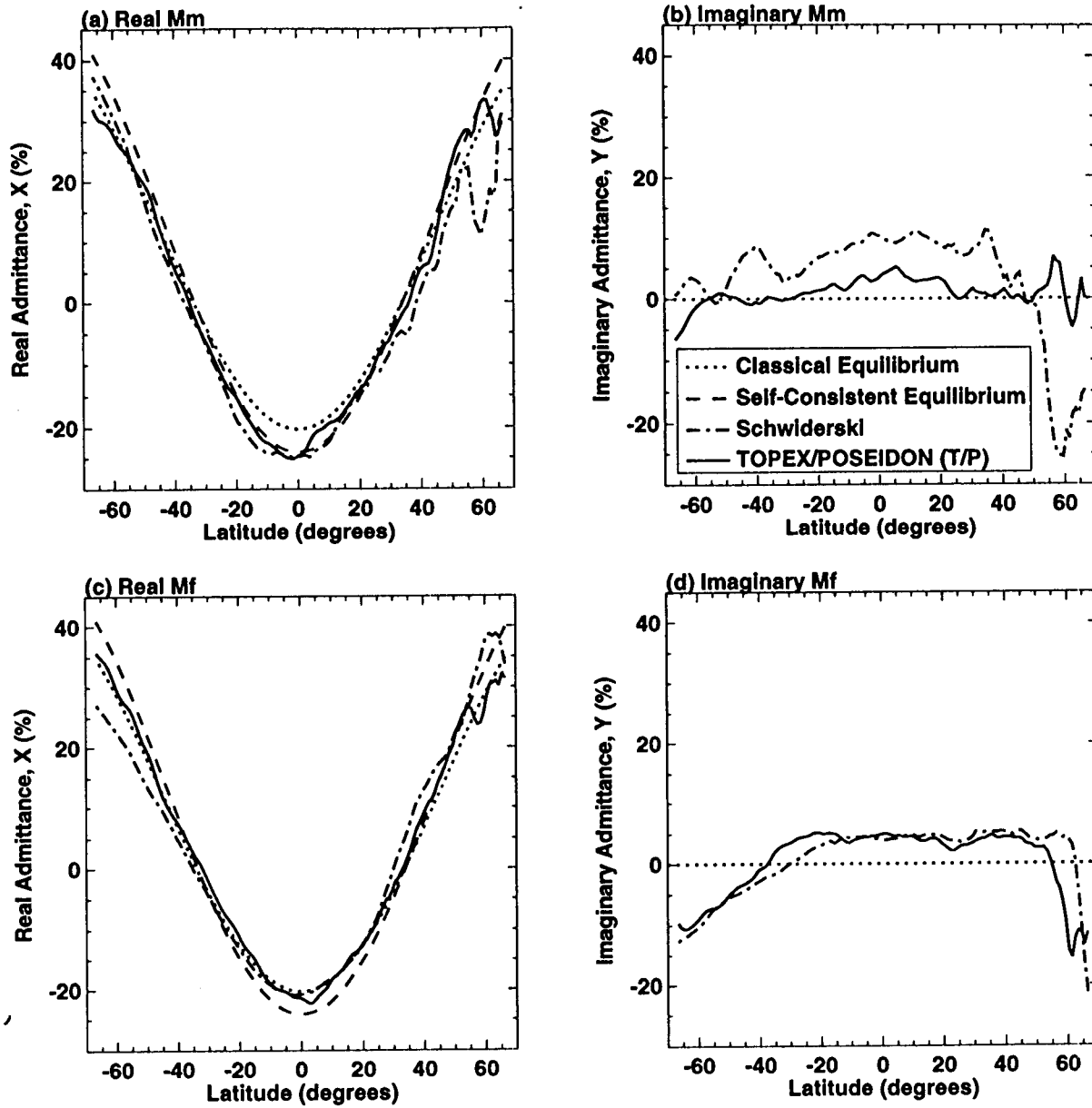


Figure 4.

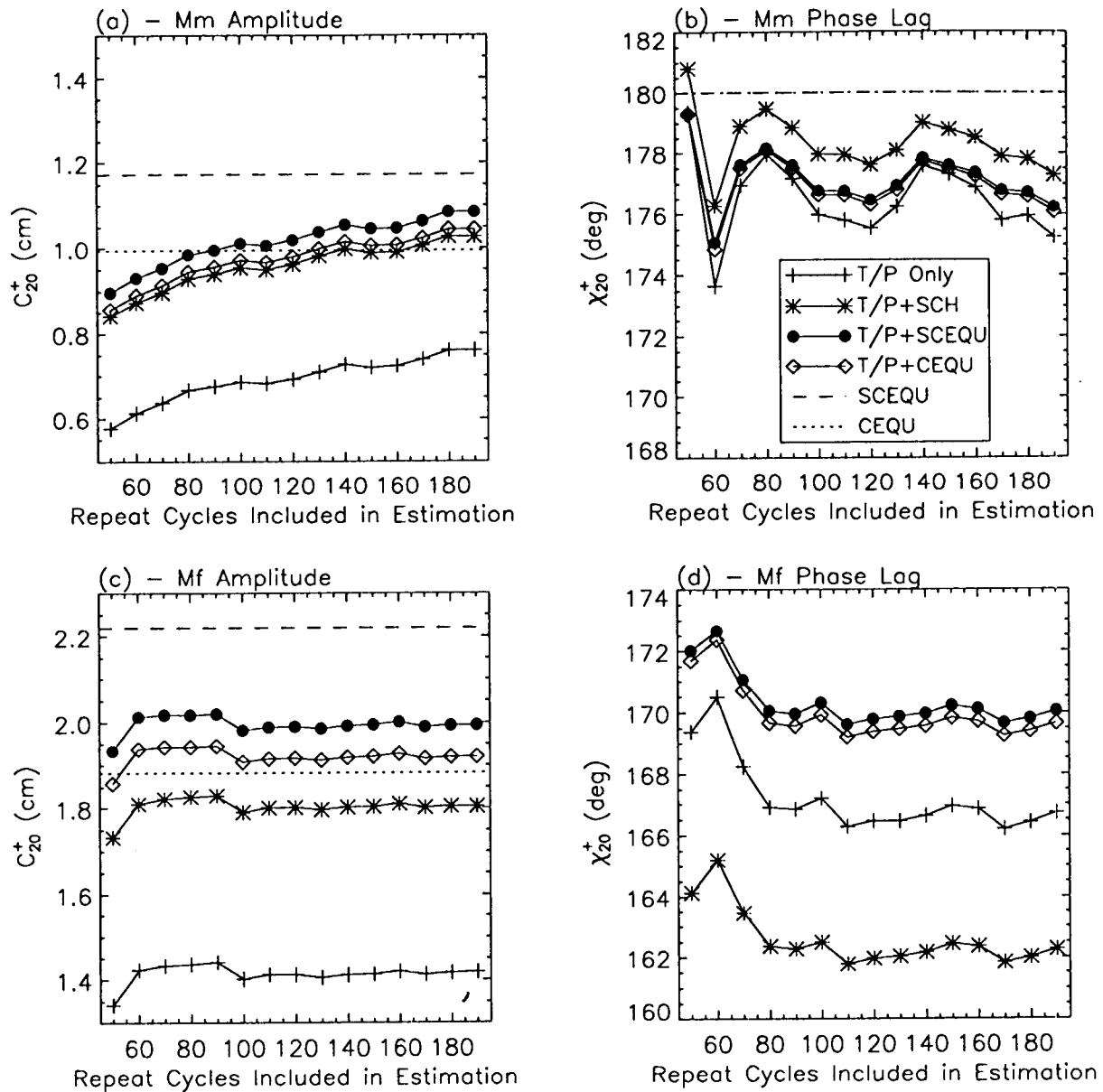


Figure 5.

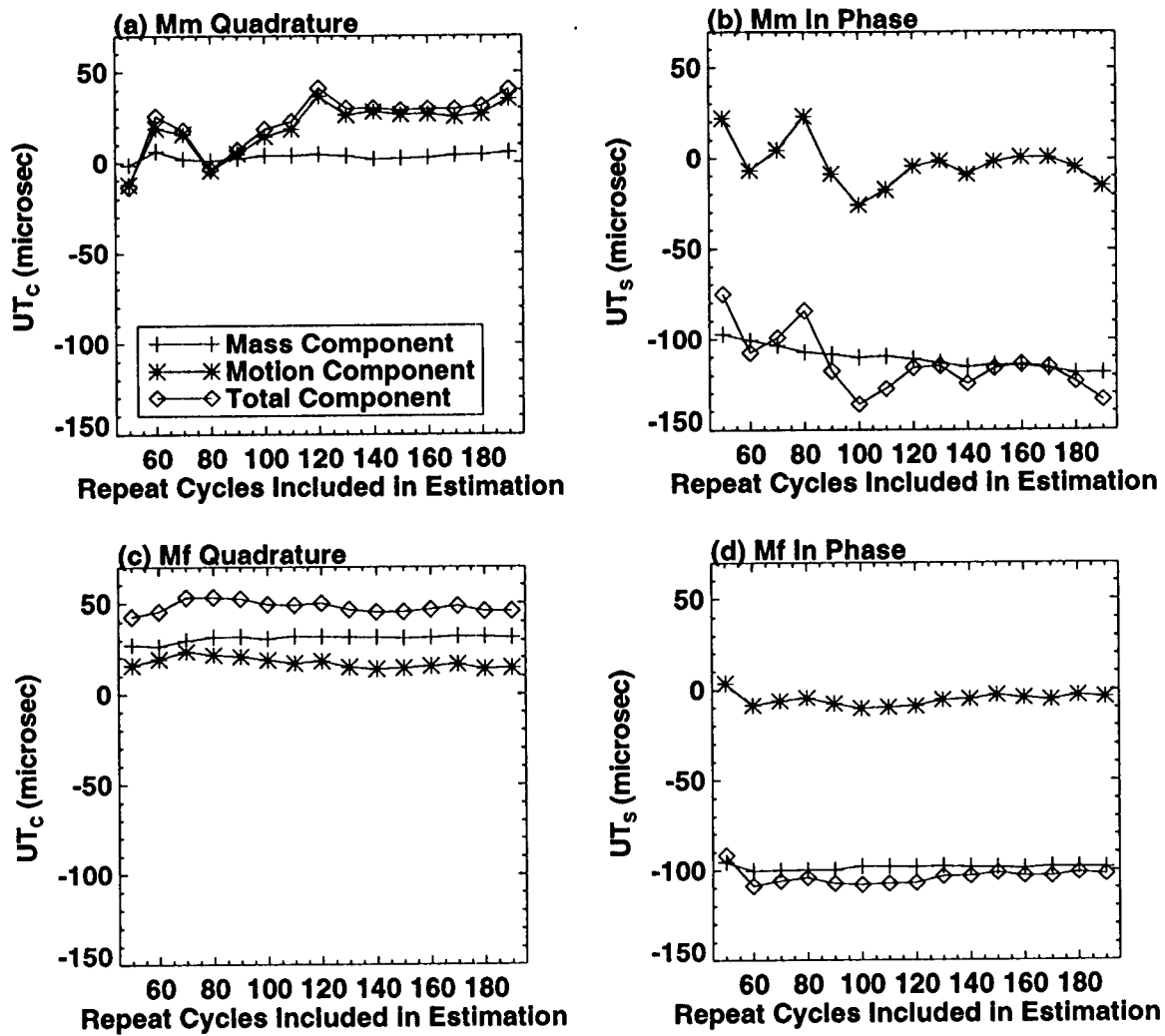


Figure 6.

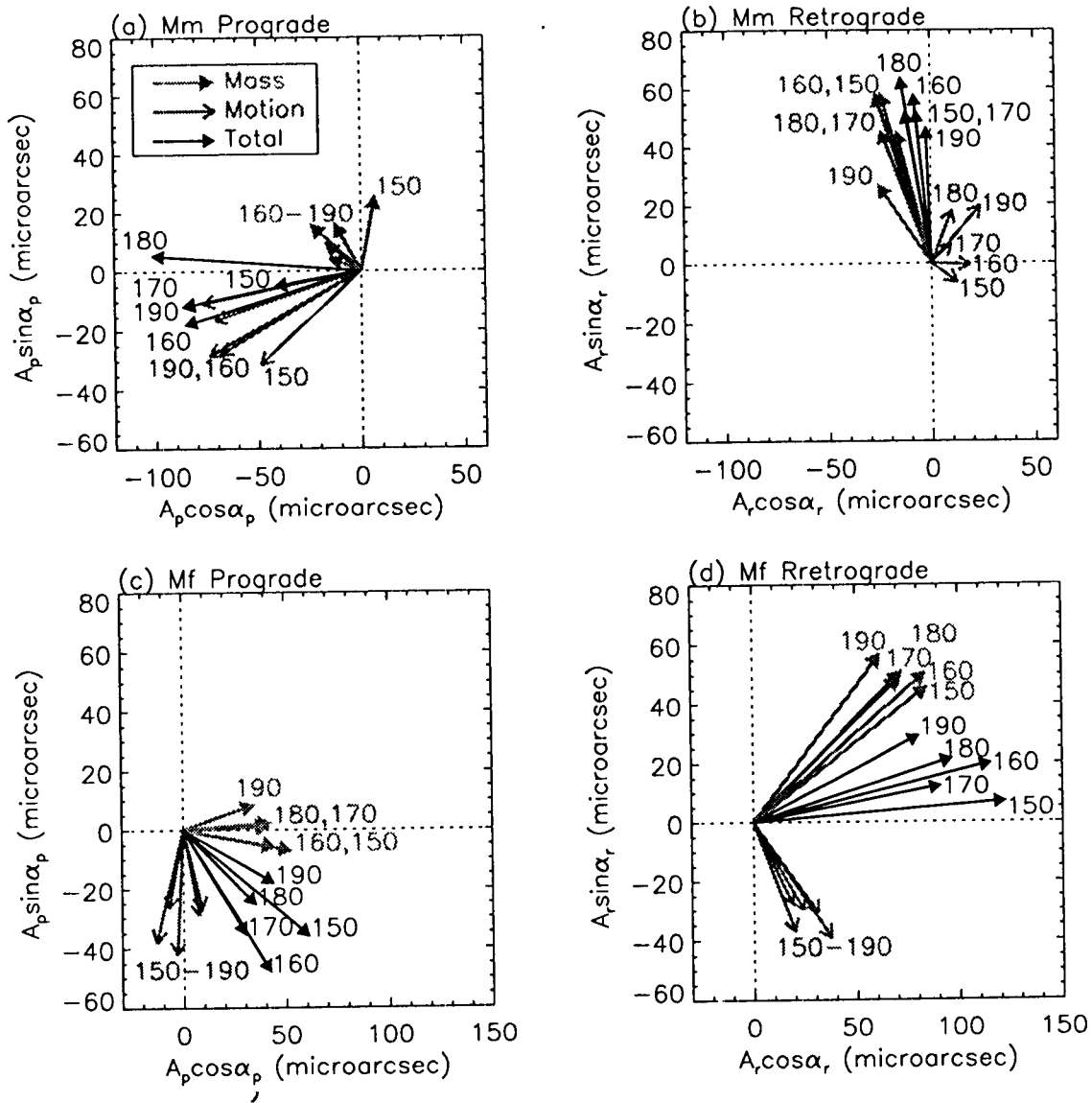


Figure 7.

